

GaAs Molecular Beam Epitaxy on (110)-Oriented Substrates

Evgeniy Klimov ¹, Aleksey Klochkov ², Sergey Pushkarev ^{1,*}, Galib Galiev ¹, Rinat Galiev ¹, Nataliya Yuzeeva ¹, Aleksey Zaitsev ³, Yuri Volkovsky ^{4,5}, Alexey Seregin ^{4,5} and Pavel Prosekov ^{4,5}

¹ Mokerov Institute of Ultra High Frequency Semiconductor Electronics, Russian Academy of Sciences, Moscow 117105, Russia

² Institute of Nanoengineering in Electronics, Spintronics and Photonics, National Research Nuclear University “MEPhI”, Moscow 115409, Russia

³ Nanotechnology in Electronics, National Research University of Electronic Technology “MIET”, Moscow 124498, Russia

⁴ Shubnikov Institute of Crystallography, Federal Scientific Research Centre “Crystallography and Photonics”, Russian Academy of Sciences, Moscow 119333, Russia

⁵ National Research Centre “Kurchatov Institute”, Moscow 123182, Russia

* Correspondence: s_s_e_r_p@mail.ru

Abstract: Molecular-beam epitaxial growth of Si-doped GaAs single-crystal layers on (110)-oriented GaAs substrates has been studied. The surface morphology of grown films was analyzed by scanning electron microscopy and atomic force microscopy, and the crystal structure of grown films was estimated by X-ray grazing incidence diffraction, in-plane pole figures, reciprocal space mapping, and photoluminescence spectroscopy. The type, concentration, and mobility of charge carriers in films were measured by the four-probe method in van der Pauw geometry at temperatures of 300 and 77 K. The possible existence of two areas in growth conditions, where increased concentration and mobility of electrons are achieved, was shown: the first, main area with the highest concentration and mobility values is $T_g = 450\text{--}500\text{ }^\circ\text{C}$ and V/III ratio $\gamma = 20\text{--}40$, the second, minor one is $T_g = 600\text{--}680\text{ }^\circ\text{C}$ and $\gamma = 40\text{--}70$. The hole conductivity was obtained at a growth temperature of $580\text{ }^\circ\text{C}$ and a low γ value of 16. It was also shown that the defect-free crystal structure of the films grown at high temperatures is not necessarily accompanied by a smooth surface.



Citation: Klimov, E.; Klochkov, A.; Pushkarev, S.; Galiev, G.; Galiev, R.; Yuzeeva, N.; Zaitsev, A.; Volkovsky, Y.; Seregin, A.; Prosekov, P. GaAs Molecular Beam Epitaxy on (110)-Oriented Substrates. *Crystals* **2023**, *13*, 28. <https://doi.org/10.3390/cryst13010028>

Academic Editor: Wolfram Miller

Received: 14 November 2022

Revised: 17 December 2022

Accepted: 19 December 2022

Published: 24 December 2022



Copyright: © 2022 by the authors. Licensee MDPI, Basel, Switzerland. This article is an open access article distributed under the terms and conditions of the Creative Commons Attribution (CC BY) license (<https://creativecommons.org/licenses/by/4.0/>).

Keywords: GaAs; (110) oriented substrate; pole figures; reciprocal space mapping; amphoteric dopant; photoluminescence spectroscopy

1. Introduction

Semiconductor GaAs-based films grown on (110)-oriented GaAs substrates possess a built-in piezoelectric field [1–3]. This circumstance has a pronounced effect on the fundamental properties of the heterostructures. Such heterostructures have demonstrated promise in the production of a new generation of field-effect transistors, topological insulators, and spintronic devices [4–7]. However, epitaxial growth of GaAs layers on GaAs substrates with (110) surface orientation is much more complicated than growth on the most commonly used (100)-oriented substrates.

The arrangement of atoms on the surface of the substrate significantly affects the properties of epitaxial films. (100)-cut GaAs surface consists of surface Ga and underlayer As atoms (Ga-rich surface) or surface As and underlayer Ga atoms (As-rich surface) with double dangling bonds in both cases, whereas the surface of the GaAs (110) wafer consists of equal numbers of Ga and As atoms with single dangling bonds [8–10]. Two-dimensional layer-by-layer growth on exactly (110)-oriented GaAs substrates does not occur readily; instead, a rough surface morphology with triangular-shaped islands with a density near 10^6 cm^{-2} is usually formed [10]. The apex of these triangular islands is always points along the [001] direction [11]. The incorporation coefficient of As atoms is considerably smaller on (110)-oriented GaAs surface in contrast to (001) one [12]; on the other hand, the diffusion

length of Ga atoms on (110) surface is an order of magnitude larger than on standard (100) surface [13]. So faceting suppression can be obtained by increasing the As/Ga flux ratio γ , by lowering the growth temperature T_g , by decreasing the growth rate v_g , or by using As₂ instead of As₄ [14–18]. Growth conditions for the smooth surface of GaAs (110) layers are reported in [5] as follows: the growth temperature is 430–500 °C and the As/Ga ratio is 20–50. Moreover, the low growth rate of 0.2 monolayers per second was demonstrated to suppress the island formation and result in a terraced surface with monolayer height steps [13]. The island size and height increase and their density decrease with lowering As₄ flux at a constant growth rate and substrate temperature due to the increase of Ga adatom diffusion length [13]. The optimized growth conditions result in a smooth GaAs surface which allowed the demonstration of GaAs/AlGaAs (110) heterostructures with 2-dimensional high mobility electron gas [9,17,19–22]. The two-dimensional facets-free growth mode can be also realized by using vicinal (110)-oriented GaAs substrate tilted (1.5–6) degrees toward Ga-rich (11 $\bar{1}$) polar surface [23–26], or by using migration-enhanced epitaxy [10].

The amphoteric properties of Si atoms are most clearly manifested when doping epitaxial films on GaAs substrates with crystallographic orientations of the (110) and (n 11) A surfaces. The amphotericity coefficient of Si in GaAs defined as the acceptor-to-donor concentration ratio $[Si_{As}]/[Si_{Ga}]$ is slightly larger for the (110)-oriented substrates than for the standard (100)-oriented ones if the films are facet-free (0.22 and 0.18, correspondingly), and is twice larger if the layer surfaces are faceting [14].

A change in the type of conductivity of such films, in the case of the fixed growth temperature, is known to occur with a change in γ . So, the p -type conductivity material is obtained at small values of γ , i.e., under conditions of As deficiency, the compensated material—at medium ones, and the n -type conductivity material—at large ones [27,28]. Nevertheless, despite the intensive study of the surface morphology and behavior of Si atoms as a dopant at the (n 11)A orientations, the T_g and γ values at which the conductivity type changes are different in different works [27–31]. The same situation is typical for the (110) orientation [9,28]. The amphoteric behavior of Si atoms during the growth of Si-doped GaAs layers follows from the ability of Si atoms to be incorporated both as donors (Si_{Ga}) and acceptors (Si_{As}) in the GaAs crystal lattice. The probability for Si atoms to occupy the available As sites and to become acceptors increases if the surface coverage with As atoms decreases due to enhanced As desorption, lowered As incorporation coefficient, and decreasing flux of As molecules [8]. For this, the growth temperature should be increased, and As/Ga ratio should be lowered [28,32]. It follows from this statement, that growth conditions for achieving p -type conductivity in Si-doped GaAs films on (110)-oriented substrates substantially differ from those for obtaining a smooth surface, and the MBE growth of Si-doped GaAs layers on (110)-oriented GaAs substrate with smooth surface and in common with p -type conductivity is problematic [8]. In our previous work [33] we demonstrate that GaAs:Si epilayers grown on GaAs (110) substrates with a high concentration and mobility of charge carriers are characterized by a rough faceted surface morphology.

Thus, the optimal conditions for obtaining smooth epitaxial layers have been extensively studied, and one of the main requirements is a low growth rate of $v_g < 0.2 \mu\text{m/h}$ (0.2 ML/s). In some applications, it is required to obtain sufficiently thick epitaxial layers of more than 1 μm , when, for technological reasons, it is inconvenient to use low growth rates. Therefore, in this research we investigate the conductivity type and the electro-physical characteristics, the surface morphology, the photoluminescence spectra, and the crystal structure of uniformly Si-doped epitaxial (110) GaAs films grown at higher growth rate of 0.54 $\mu\text{m/h}$ (0.53 ML/s). We vary the growth temperature and As₄/Ga flux ratio over a wide range and determine the ranges of optimal growth conditions for obtaining a smooth GaAs (110) surface, for the highest silicon impurity activation, and for intense photoluminescence signal.

2. Materials and Methods

The samples under study were grown by molecular beam epitaxy (MBE) on a Tsna-24 setup on semi-insulating singular (110)-oriented GaAs substrates by mounting them on a molybdenum holder using indium soldering. The growth temperature T_g was measured with a thermocouple mounted behind the sample holder. Preliminary studies have shown that with this mounting, the temperature of the substrate is approximately 70 °C lower than the thermocouple readings. This is confirmed both by the analysis of PHEED patterns on the GaAs substrate (100) mounted on a molybdenum holder and by determining the sublimation temperature of GaAs. When the substrate was heated to 720 °C in an arsenic-free atmosphere, we observed the development of surface roughness, which was visible as metallic droplets in an electron microscope. In the following, all temperatures correspond to the nominal readings of the thermocouple. The RHEED analysis of the investigated samples was problematic due to the small size of the substrate pieces in the holder.

The pregrowth annealing of the substrates was carried out in the growth chamber in an As₄ flow at temperatures up to 680 °C. After that, an undoped GaAs buffer layer 135 nm thick and a silicon-doped GaAs:Si layer 675 nm thick were grown at the same temperature T_g . The growth conditions for all studied samples are shown in Table 1. The samples were grown at different T_g values from 410 to 680 °C. The ratio of the partial pressures of arsenic tetramers P_{As_4} and gallium atoms P_{Ga} in the growth zone ($\gamma = P_{As_4}/P_{Ga}$) was varied in the range of 14–84. The growth rate was $v_g = 90 \text{ \AA}/\text{min}$ (0.53 ML/s). The growth conditions for the buffer and the silicon-doped GaAs layers were the same for every sample. The temperature of the silicon cell was 1080 °C for all samples, which corresponded to a concentration of conduction electrons of $1 \times 10^{18} \text{ cm}^{-3}$ under standard growth conditions on GaAs (100) substrate at $v_g = 90 \text{ \AA}/\text{min}$ (0.53 ML/s).

Table 1. Growth conditions (growth temperature T_g , and As₄/Ga flux ratio γ) and properties of Si-doped GaAs (110) films (electron or hole conductivity, carrier mobility μ , and concentration n , root mean square surface roughness R_q).

Sample #	$T_g, \text{ }^\circ\text{C}$	γ	Carriers	$\mu, \text{ cm}^2/(\text{V}\cdot\text{s})$		$n, \text{ cm}^{-3}$		$R_q, \text{ nm}$
				300 K	77 K	300 K	77 K	
72	410	55	–	–	–	–	–	5.2
71	460	53	electrons	230	–	4.5×10^{16}	–	5.8
91		14	electrons	300	100	2.8×10^{17}	3.0×10^{17}	13.9
88	480	24	electrons	620	490	3.7×10^{17}	3.8×10^{17}	8.0
84		42	electrons	1140	895	4.3×10^{17}	4.5×10^{17}	3.6
90		84	–	–	–	–	–	7.8
70	510	46	electrons	230	100	1.3×10^{17}	1.4×10^{17}	8.5
83	550	42	electrons	430	360	3.5×10^{17}	3.6×10^{17}	15.3
87		16	holes	51	77	4.3×10^{17}	1.1×10^{17}	117
75	580	25	–	–	–	–	–	12.3
73		58	electrons	1040	850	2.5×10^{17}	2.5×10^{17}	15.5
76		80	–	–	–	–	–	21.9
74	620	58	electrons	2390	2130	5.6×10^{17}	5.6×10^{17}	11.1
80	680	44	electrons	690	560	3.9×10^{17}	3.9×10^{17}	51.3

The electrophysical characteristics (mobility and concentration of charge carriers) were determined by measuring the resistivity and the Hall effect by a four-probe method in van der Pauw geometry at temperatures of 300 and 77 K in the dark. The photoluminescence (PL) spectra were measured in a combined optical cryostat at 77 K. The PL emission was excited by focused radiation of a solid-state laser with a wavelength of 409 and 532 nm

and a power of 200–300 mW and was detected in the photon energy range of 1.2–2.0 eV by photoelectron multiplier FEU-62 cooled with liquid nitrogen. The energy resolution of the PL setup was 5 meV.

The surface roughness of the samples was measured on an NT-MDT Solver Pro atomic force microscope (AFM) in the contact mode. The root mean square (RMS) surface roughness R_q was calculated over a field of $10 \times 10 \mu\text{m}$. Moreover, the surface of the samples was examined in a Raith-150 Two setup in a scanning electron microscope (SEM) mode with an electron energy of 10 keV.

X-ray diffraction studies of the samples were carried out on a SmartLab Rigaku X-ray diffractometer using a 9-kW rotating anode molybdenum $K_{\alpha 1}$ radiation source with wavelength $\lambda = 0.70930 \text{ \AA}$.

3. Results and Discussion

3.1. Surface Roughness

Table 1 lists the samples with growth temperature and γ , as well as RMS surface roughness. The investigated samples can be grouped into three series: (i) 4 samples with $T_g = 480 \text{ }^\circ\text{C}$ and various γ , (ii) 4 samples with $T_g = 580 \text{ }^\circ\text{C}$ and various γ , (iii) 8 samples synthesized at different growth temperatures, and close V/III-ratios of $\gamma = 40\text{--}60$. It is useful to compare film properties as a function of T_g or γ in these sample series.

SEM images of the surface of samples formed at various substrate temperatures and arsenic pressures $\gamma = 40\text{--}60$ are given in Figure 1. The smoothest surface at given γ is observed for samples # 71 and # 84 obtained at temperatures of 460 and 480 $^\circ\text{C}$. As the growth temperature decreases, a wavy surface is obtained. With an increase in the growth temperature to 510–580 $^\circ\text{C}$, the surface contains pits and hills. With a further increase in temperature above 620 $^\circ\text{C}$, the formation of faceted pyramidal features oriented along the [001] surface direction occurs.

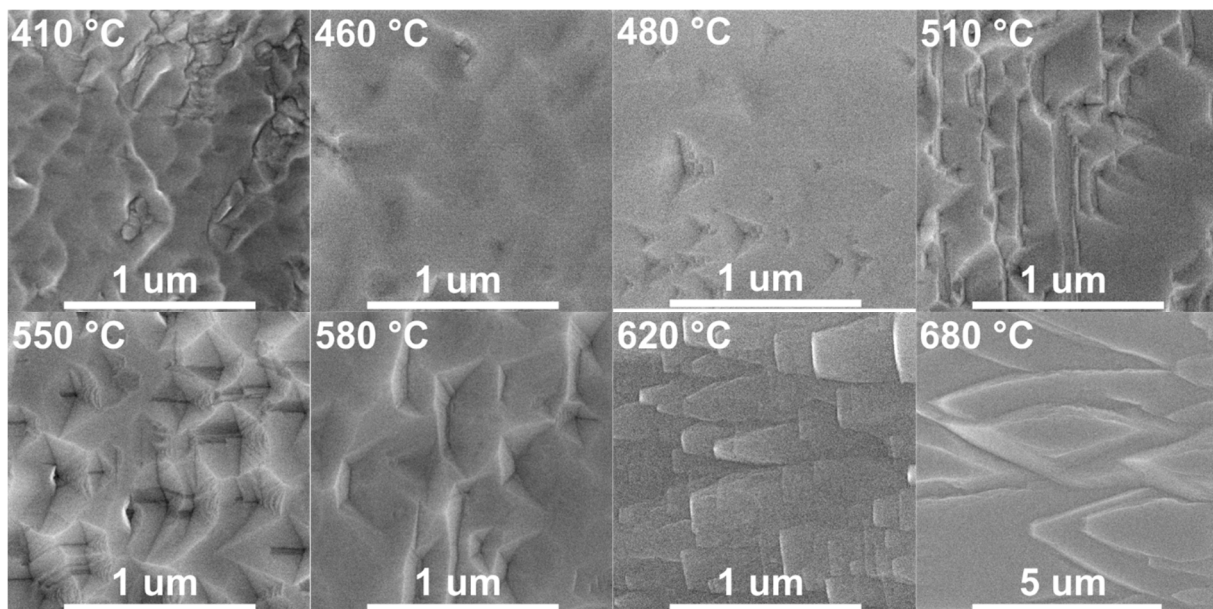


Figure 1. SEM of GaAs:Si (110) films formed at different growth temperatures and $\gamma = 40\text{--}60$.

Height maps of the surface of the samples measured by AFM are shown in Figure 2. As follows from Table 1, a series of samples obtained at a temperature of 480 $^\circ\text{C}$ has the lowest roughness. For low growth temperatures, triangular pits are the main type of surface defects. The density of pits is minimal at arsenic flux overpressure in the range of about $\gamma = 42\text{--}58$ and rises with both decreasing and increasing arsenic fluxes.

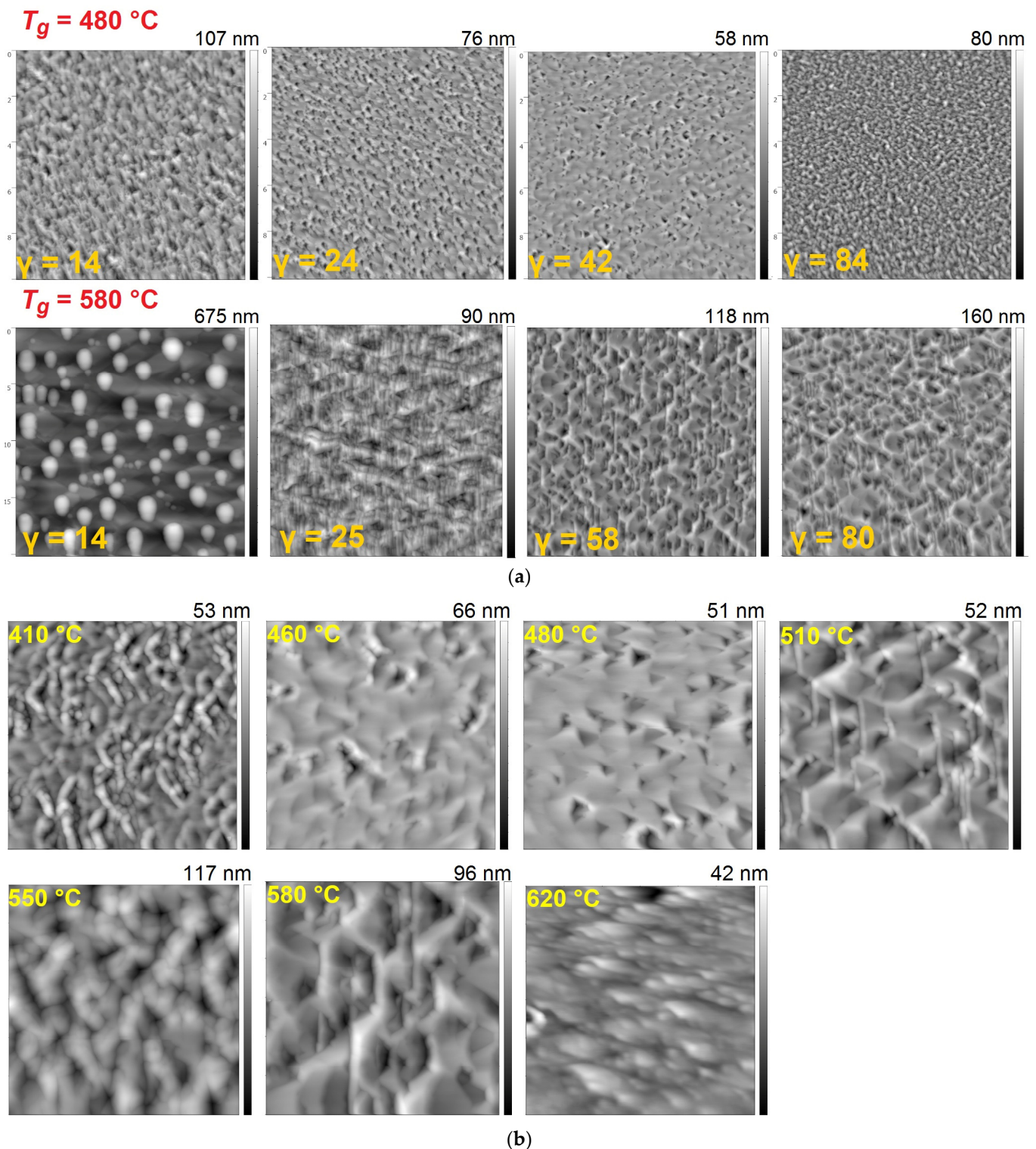


Figure 2. AFM surface maps of GaAs:Si (110) films: (a) $10 \times 10 \mu\text{m}^2$ scans for films formed at $T_g = 480$ and 580 °C with different As_4 fluxes; (b) $3 \times 3 \mu\text{m}^2$ scans for films grown with different substrate temperature at $\gamma = 40$ – 60 . The range of the color scale z is indicated above it.

At $T_g = 580$ °C, a more significant dependence of the surface roughness on the arsenic flux is observed. With an increase in γ , a change in the growth regime from a lack of arsenic to its excess is observed. At low $\gamma = 14$, a film with an RMS surface roughness of 117 nm was obtained due to large spherical drops of gallium. At $\gamma > 25$, arsenic flux is sufficient to

form GaAs, and a rough faceted surface with predominant crystallographic orientations is observed.

At $T_g = 620\text{ }^\circ\text{C}$, hills elongated along the surface direction [001] are formed. With a further increase in growth temperature to $680\text{ }^\circ\text{C}$, the size of the hills becomes macroscopic, so they become easy to observe in an optical microscope.

Due to the sufficient amount of experimental data, it can be visualized in the form of a 3D color map surface with the help of interpolation based on the thin plate spline (TPS) algorithm. This method assumes that all the data points are distributed on a thin elastic plate which is constrained at the grid points and forms a two-dimensional surface by spanning the grid points. The surface is deformed between the points to form a likely fit to the data. The best results are generally found by minimizing the bending energy of the plate. Figure 3 demonstrates the possible variation of RMS surface roughness in the whole range of used growth conditions. Analysis of Figure 3 reveals the following dependencies: firstly, surface roughness tends to increase with increasing growth temperature; secondly, surface roughness tends to increase at the edges of the used range $\gamma = 40\text{--}60$. The growth conditions for smooth surfaces reported in [23] are in good agreement with our experiment.

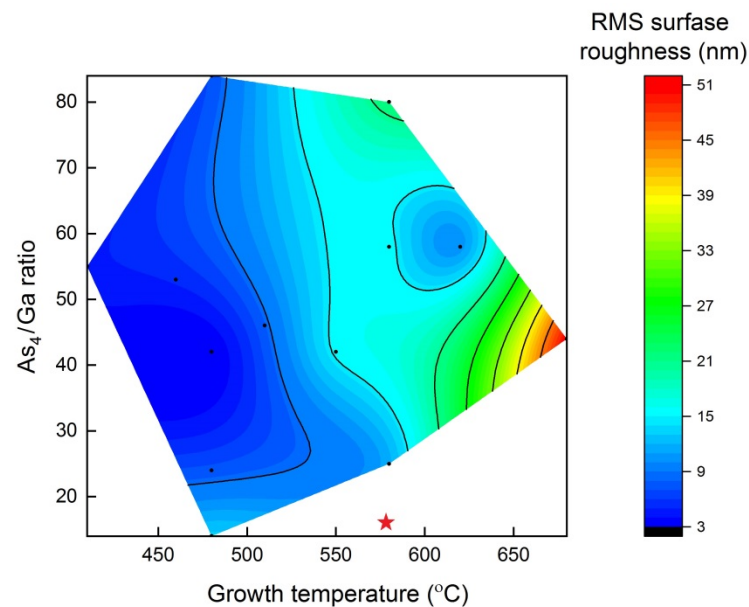


Figure 3. Root mean square roughness vs. growth temperature and As_4/Ga ratio (black dots are experimental measurements, out-of-order sample #87 with hole conductivity and with extra-large surface roughness 117 nm is marked by asterisk outside the interpolation area).

3.2. Conductivity

In order to check the quality of the i-GaAs buffer layer, additional structures were grown in the form of undoped GaAs layers 135 nm thick. The pregrowth preparation of the substrates and the growth conditions for such additional structures corresponded to the samples under study. The growth temperatures were 480, 510, 540, and $580\text{ }^\circ\text{C}$. Hall measurements have shown that the buffer layers are highly resistive regardless of the preparation conditions. Thus, undoped buffer layers obtained at different temperatures did not contribute to the measured concentration and mobility of charge carriers for the samples shown in Table 1.

The concentration of charge carriers depends on the growth conditions and is in the range of $(1.3\text{--}5.6) \times 10^{17}\text{ cm}^{-3}$. The charge carrier concentration is temperature-independent. The electron mobility in the samples is less at 77 K than that at the room temperature. Moreover, the electron mobility values are significantly lower than the values that are usually obtained for *n*-type GaAs films grown in substrates with standard (001) orientation at optimal growth conditions. This indicates a high concentration of scattering centers in the synthesized GaAs (110) films, which depends on the growth temperature and, in our

case, is minimal at $T_g = 680$ °C. The mobility of electrons in a cooled sample decreases due to the fact that the dominant mechanism of charge carriers scattering is scattering on defects and ionized impurities, and not on phonons. It is well known that as the temperature of the sample decreases, this type of scattering increases. As for the electron concentration, it should be taken into account that the cooled samples react much more strongly to unintentional illumination during measurements: photoexcited electrons recombine with a noticeable time delay and contribute to the measured concentration. We have often observed this effect; it can be neutralized by carefully darkening the room in which the Hall setup is located.

Table 1 shows that GaAs:Si (110) films have *n*-type conductivity at growth temperatures $T_g > 460$ °C and average values of arsenic overpressure $\gamma = 40$ –60 (as it was reported in [33]). It should be noted that the type, mobility, and concentration of charge carriers in the case of substrate orientation (110) are functions of the flux of arsenic molecules. Thus, for a series of four samples grown at $T_g = 480$ °C, the concentration and mobility of electrons increase monotonically with an increase in γ from 14 to 42. Nevertheless, sample # 90 grown with $\gamma = 84$ is non-conductive. In a series of samples grown at $T_g = 580$ °C, there is a transition from *p*-type conductivity (sample # 87) at low $\gamma = 16$ to *n*-type conductivity with an increase in γ to 58 (sample # 73). In this case, sample # 75 grown at intermediate $\gamma = 25$, and sample # 76 with a high value of $\gamma = 80$ are semi-insulating.

Thus, the electrophysical properties of epitaxial GaAs: Si (110) films substantially depend on the growth conditions: at each fixed growth temperature, there is a narrow γ range, in which *n*-type films with high electron concentration and mobility are obtained. With a decrease in γ , Si atoms begin to occupy acceptor sites in the GaAs crystal lattice. Therefore, with a decrease in γ , the conductivity type of GaAs: Si films changes from *n*-type to *p*-type through a nonconducting compensated state. When γ rises to 80, GaAs:Si (110) films grown at $T_g = 480$ and 580 °C become non-conductive. A possible explanation is that the As excess causes the formation of antisite As_{Ga} defects, which cause a shift of Fermi level to the midgap and, therefore, the drop in the electron density [34]. The range of optimal γ for samples with *n*-type conductivity is most likely a function of the growth temperature. Thus, a decrease in the concentration and mobility of electrons is observed in sample # 80, obtained at a high growth temperature $T_g = 680$ °C, in comparison with sample # 74 ($T_g = 620$ °C)

The experimental data are visualized in form of a 3D color map surface with the help of interpolation based on the TPS algorithm. Figure 4 demonstrates the variation of carrier concentration and mobility in the whole range of used growth conditions. The interpolation reveals the probable existence of two areas of growth conditions where increased values of the concentration and mobility of electrons are achieved: the first area is $T_g = 450$ –500 °C and $\gamma = 20$ –40, the second one is $T_g = 600$ –680 °C and $\gamma = 40$ –70. An increase in the optimum arsenic pressure for efficient electron doping is also observed with increasing temperature. Note that there is a correlation between electron concentration and electron mobility: on average, the higher values of the electron concentration correspond to the higher values of their mobility, and vice versa (Figure 5). Since the concentration of doping Si atoms is the same in all samples, the observed effect indicates different concentrations of compensating and scattering centers in the samples. Note that the growth conditions from the first optimal area ($T_g = 450$ –500 °C and $\gamma = 20$ –40) make it possible to obtain films with a smoother surface.

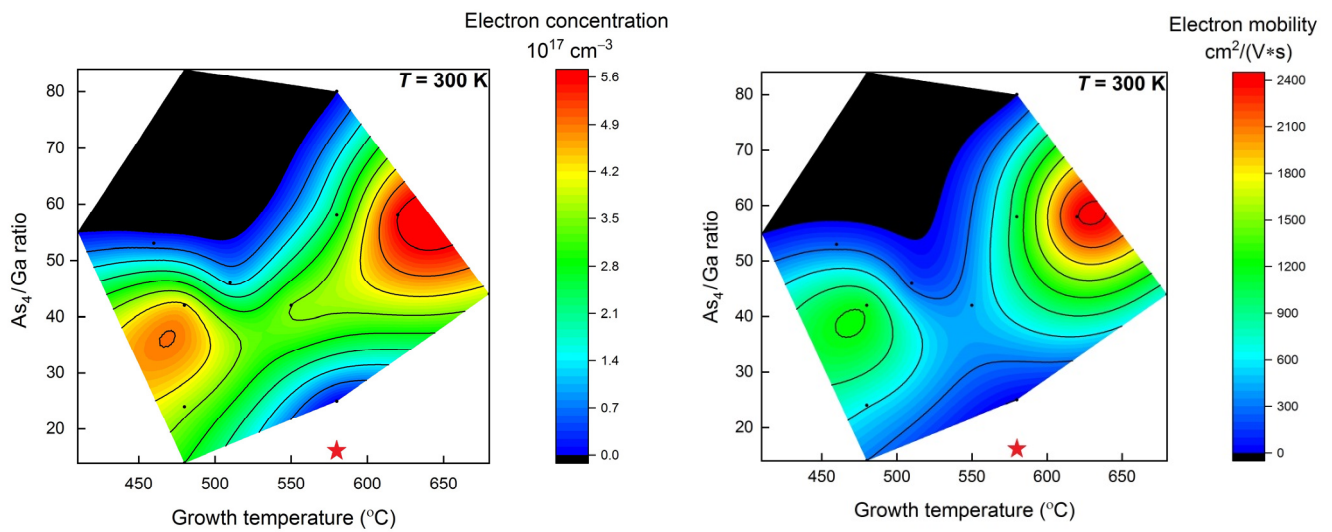


Figure 4. Electron concentration and mobility vs. growth temperature and As_4/Ga ratio (black dots are experimental measurements, values of n and μ are conventionally considered zero for non-measurable samples with too low conductivity, out-of-order sample #87 with hole conductivity is marked by asterisk outside the interpolation area).

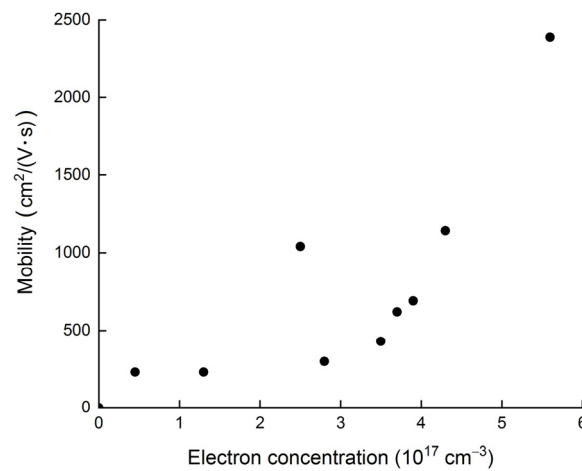


Figure 5. Correlation between electron mobility and its concentration (sample # 87 with hole conductivity is excluded).

3.3. Photoluminescence Spectroscopy

The PL spectrum of the investigated samples is presented at Figure 6; samples are grouped into three series as in Section 3.1. The spectrum of Si-doped GaAs (110) film contains three peaks in the photon energy range of 1.25–1.60 eV. The high energy peak with a maximum at $\hbar\omega_1 = 1.51$ –1.52 eV inherent in all the samples refers to the edge PL of GaAs. In spite of expectation, the energy position of this peak is not unambiguously correlates with the concentration of charge carriers. The bands of optical transitions at $\hbar\omega_2 = 1.40$ –1.45 eV which is also inherent in all the samples and $\hbar\omega_3 = 1.25$ –1.33 eV which is absent or too low-intensive in some spectra are related to impurity PL. In accordance with [35,36], it is thought that the V_{Ga} and V_{Ga} defects are responsible for the PL peak at 1.4 eV. The PL signal at $\hbar\omega_2 = 1.40$ –1.45 eV is most probably associated with V_{As} defects for samples grown at a small value of γ , and with V_{Ga} defects for samples grown at a high value of γ . The V_{Ga}^- and V_{Ga}^{2-} defects appear as peaks in the PL spectra at the energies $\hbar\omega_3 = 1.25$ –1.33 eV.

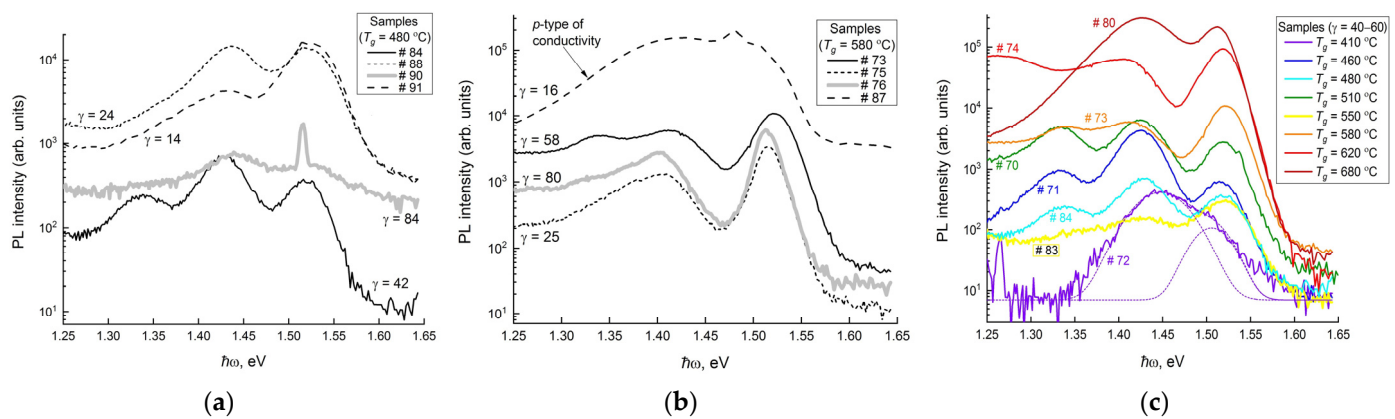


Figure 6. PL spectra: (a) samples grown at 480 °C; (b) samples grown at 580 °C; (c) samples grown at intermediate V/III ratio $\gamma = 40\text{--}60$ (the γ values are marked near all the curves, the growth temperature T_g is shown in colors, sample #87 with holes is marked by an arrow, spectrum of sample #72 is decomposed on the two Gaussians for visualizing).

Sample #87 with *p*-type conductivity demonstrates PL spectrum is radically different in shape from the PL spectra of other samples: the prevailing band lies at 1.48 eV, whereas the high energy band manifests itself as a clearly pronounced shoulder at 1.505 eV. In the case of the (*n*11)A orientation, the feature observed at 1.48 eV is commonly attributed to the transitions of electrons from the conduction band to the Si_{As} level and to the $\text{Si}_{\text{Ga}}\text{--}\text{Si}_{\text{As}}$ transitions [27,36]. We also can conceive that the 1.48 eV PL peak in sample #87 is defined by the transitions from the conduction band to the Si_{As} levels and by $\text{Si}_{\text{Ga}}\text{--}\text{Si}_{\text{As}}$ transitions.

3.4. X-ray Diffraction

3.4.1. Comparative Study of Surface Roughness between Samples

Studies of samples carried out by AFM method showed that the values of their surface roughness vary from 5 to 50 nm (#84 – 5 nm, #83 – 15 nm, #80 – 50 nm; see Table 1). However, the area of surface scanning during AFM measurements usually does not exceed several tens of square microns. X-ray methods can be used to study the whole sample surface. It is a difficult task to apply widely used X-ray reflectivity and power spectral density analysis methods when studying surfaces with a roughness of tens nm. Therefore, we apply the X-ray grazing incidence diffraction (GID) or in-plane XRD method to compare surface roughness between samples. The beam in this method is directed at a small angle to the surface near the total external reflection region. In this geometry, the diffraction (scattering) plane is close to the sample surface and diffraction reflection is recorded from the Laue crystal planes. These crystal planes are perpendicular to the sample surface. The penetration of X-rays with respect to the surface normal under the total external reflection conditions (Λ —extinction depth) is several nanometers. The intensity of the diffraction peak in this geometry will strongly depend on the surface relief. Inhomogeneities and imperfections of the layer within the extinction depth will lead to a decrease in the intensity of the diffraction reflection. Moreover, if we assume that the surface relief of the samples is uniform in the lateral plane, then the ratio of the surface roughness to the thickness of the layer in which the diffraction reflection is formed will determine the intensity of the diffraction peak.

Figure 7 shows the experimental diffraction peaks of the reflection (004) obtained by the GID method for samples #80, #83, #84. A comparison of the integrated intensity reflected from plane (004) shows that the peak from sample #84 has the maximum intensity, the peak of sample #83 is less bright, and the peak of sample #80 has the minimum intensity. The calculated value of the extinction depth of Mo $K_{\alpha 1}$ radiation in GaAs is about 5 nm. It can be assumed that the roughness averaged over the sample surface for samples #83 and #80 significantly exceeds the extinction depth. Sample #84 has the smoothest surface and

its surface roughness is comparable to the extinction depth. This is in good agreement with the local values of roughness obtained by the AFM method.

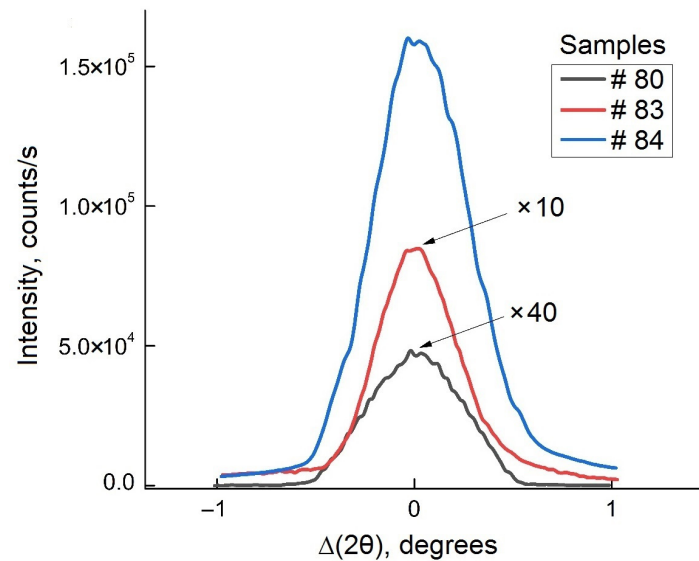


Figure 7. Experimental GID curves of (004) reflection for samples #80, #83, #84. For clarity, the intensities of peaks #83 and #80 are multiplied by 10 and 40, respectively.

3.4.2. Determination of the Degree of Crystallinity of Films

In this paper, we used the in-plane pole figure (PF) method to determine the degree of crystallinity of films. This method is based on the construction of the distribution of the intensity diffracted by the sample similar to the gnomostereographic projection for a given crystallographic orientation in the grazing incidence geometry.

Figure 8 shows the in-plane PF of (004) reflections for samples #80, #83, #84. The ND direction (normal to the plane of the figure in the center of the PF) corresponds to the normal to the film surface. The circles mark the position of the main reflections corresponding to the [100], [010], [001] directions of the film in the case of a perfect structure (in accordance with the theory). It can be seen from Figure 8 that, in addition to the main peaks, there are additional reflections, which indicates the presence of misoriented crystal blocks. The presence of grains and the domain structure of the film can be assumed.

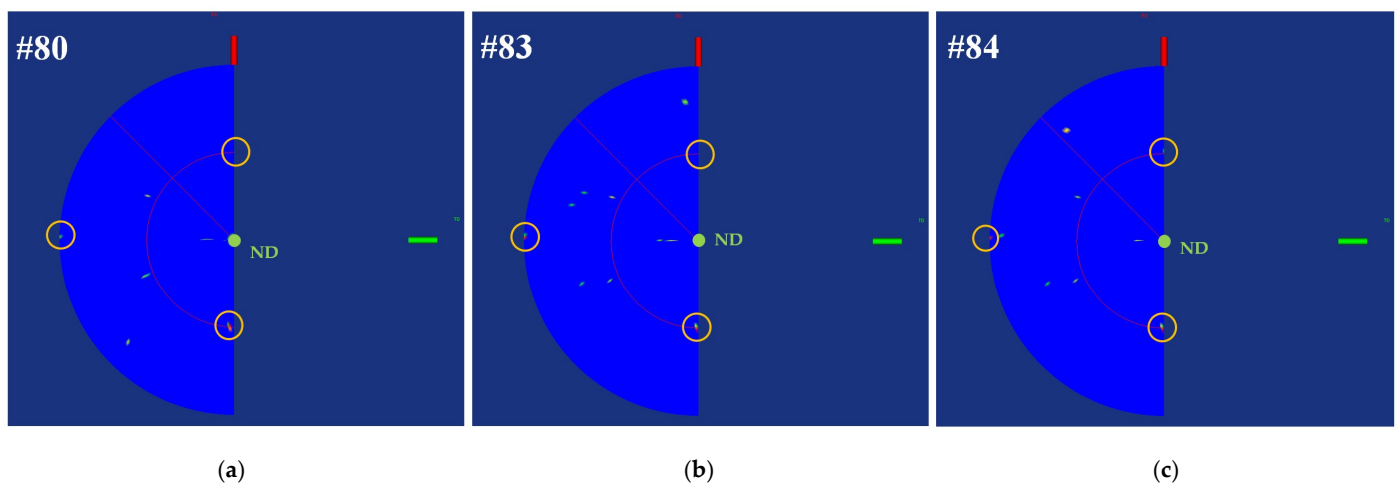


Figure 8. In-plane pole figures of (004) reflections for samples #80 (a), #83 (b), #84 (c). The ND direction presented (a normal to the drawing plane in the PF center) corresponds to a normal to a film surface. Yellow circles noted the provision of the main reflexes 400, 040, 004 in case of perfect structure (according to the theory).

The shape of both the main and additional reflections are point, they do not show blur (which is typical for textures) and not in the form of stripes (which is typical for a polycrystal). This allows us to make the assumption that the film in all samples is monocrystalline.

A comparison of the experimental PFs (Figure 8) shows that sample #80 (Figure 8a) has a more perfect structure. Since it has a minimal number of additional reflections in comparison with samples #83 (Figure 8b) and #84 (Figure 8c).

3.4.3. Determination of the Real Crystal Structure

Reciprocal space mapping (RSM) was used to obtain information about the real structure of the films. This method is based on the registration of scattering maps near the reciprocal lattice point of a given reflection using a three-crystal high-resolution X-ray diffractometry scheme.

Figure 9 presents the experimental RSMs for samples #80, #83, #84 near the (220) reciprocal lattice point. A separate diffraction peak (220) from the epitaxially synthesized GaAs:Si layer is not observed. Since by the method of pole figures we found out that the layer is crystalline, it can be assumed that the normal lattice parameter coincides with the substrate parameter within the diffraction conditions for (220) reflections of the substrate.

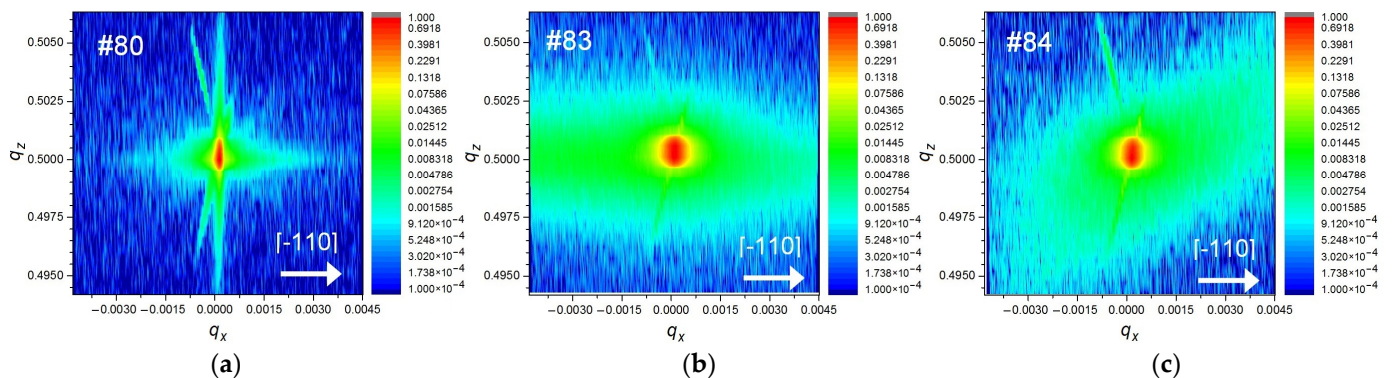


Figure 9. The experimental RSMs for the samples #80 (a), #83 (b), #84 (c) near the (220) reciprocal lattice point. The arrow marks the crystallographic direction $[\bar{1}10]$ (according to the direction of the base cut, which was indicated by the arrow on the samples). The intensity is normalized to the peak intensity for each of the RSMs.

The RSM of the studied samples #80, #83, #84 differ significantly. The major difference appears in the form and intensity of diffuse scattering, which occurs due to scattering at the crystal structure defects. Diffuse scattering in sample #80 is very small, which means that scattering by defects in the crystal structure is just as small in comparison with samples #83, #84.

Diffuse scattering in samples #83, #84 is approximately the same in magnitude and significantly exceeds the scattering in sample #80. In this case, the shape of scattering in samples #83, #84 also differs from each other. In sample #83 (Figure 9b) the diffuse scattering “halo” is elongated horizontally, along the q_x axis (along the crystallographic direction $[\bar{1}10]$). In sample #84 (Figure 9c) the distribution of the intensity of diffuse scattering has the shape of an ellipse located with the larger axis along a straight line making an angle of about 20–30° with the direction of the q_x axis.

According to the AFM and X-ray reflectivity data, sample #80 has the greatest surface roughness, sample #83—medium, #84—the lowest surface roughness among the samples (see Table 2). The sample with the greatest roughness demonstrates the smallest diffuse scattering by defects in the crystal structure, which is probably because sample #80 has a more perfect structure among the test samples. Samples #83 and #84 with the average and lowest roughness values showed more scattering at structural defects, and the layer structure in these samples seems more defective. In sample #84 with the smallest value of roughness, diffuse scattering has a specific character, which most likely indicates the

presence in the layer of a certain (predominant) type of structural defect. In addition, these samples demonstrate the coincidence of trends in the intensity of PL emissions, which depend on the concentration of point defects—PL quenchers (as seen in Figure 6c)—and the intensity of XRD diffuse scattering (see Figure 6c)

Table 2. Features of crystal structure and defectiveness degree of samples 80, 83, 84.

Sample	T_g , °C	γ	R_{q_r} , nm	(004) XRD Reflection		μ , cm ² /(V·s)	n , $\times 10^{17}$ cm ⁻³	Number of Additional Reflections	Diffuse Scattering
				Intensity, counts/s	FWHM, °				
# 80	680	44	51	1 154	0.556	690	3.9	4	low
# 83	550	42	15	8 464	0.478	430	3.5	8	high
# 84	480	42	3.6	159 260	0.563	1140	4.3	6	medium

It is important to note that broadening the diffraction peak of the substrate along the q_x axis (near the center of the RSM) is observed in samples #83 and #84, which is not observed in sample #80. This is also probably due to additional scattering by defects in the crystal structure of samples # 83, #84.

4. Conclusions

The growth of Si-doped GaAs layers on (110)-oriented GaAs substrates by means of molecular-beam epitaxy has been studied. Faceted pyramidal features oriented along the [001] direction appear on the surface of the film as the growth temperature increases. Surface roughness is shown to be monotonically sufficiently increased with growth temperature increase in the range of 410–680 °C, while a change of As_4/Ga flux ratio γ in the range of 14–84 leads to a lowering of surface roughness at intermediate values of 30–60. An exception is the growth regime leading to p -type conductivity ($T_g = 580$ °C and $\gamma = 16$); in this case, the film has an abnormally high roughness. The interpolation of Hall measurement results reveals the probable existence of two areas in growth conditions where increased concentration and mobility of electrons are achieved: the first, main area with the highest concentration and mobility values is $T_g = 450$ – 500 °C and $\gamma = 20$ – 40 , the second, minor one, is $T_g = 600$ – 680 °C and $\gamma = 40$ – 70 . The films synthesized with parameters in the first optimal area have smoother surfaces than films synthesized with other optimal parameters. As mentioned, the GaAs:Si layer with hole conductivity was obtained when growing it in GaAs (110) substrate at 580 °C and low $\gamma = 16$.

Measurements of the XRD in-plane pole figures showed that the grown GaAs (110) layers are generally single crystals, but with different defect concentrations. Defects of crystal structure generated in lower temperature growth regimes lead to more diffuse X-rays scattering which becomes apparent in reciprocal space mapping of X-rays scattering. Films with defective crystal structure and low PL emission possess smoother surfaces and higher electron mobility, whereas films with more perfect crystallinity and higher PL emissions have rougher surfaces. This suggests that different types of defects in the crystal structure impact the electrical properties of the samples in different ways; X-ray and photoluminescence studies have different sensitivity to them. The ratio of different types of defects is governed by the conditions of MBE growth; however, a deeper investigation is not available within the framework of this research.

Author Contributions: Conceptualization, G.G.; methodology, G.G. and E.K.; software, A.K.; validation, S.P.; formal analysis, N.Y.; investigation, A.K., A.Z., Y.V. and A.S.; resources, E.K.; data curation, A.K. and P.P.; writing—original draft preparation, S.P. and P.P.; writing—review and editing, A.K., E.K. and P.P.; visualization, S.P. and R.G.; supervision, G.G.; project administration, E.K.; funding acquisition, E.K. All authors have read and agreed to the published version of the manuscript.

Funding: The study was funded by the Russian Science Foundation grant No. 22-19-00656, <https://rscf.ru/en/project/22-19-00656/> (accessed on 14 November 2022). The part of the research

carried out by Yu. A. Volkovsky and P.A. Prosekov was supported by the Ministry of Science and Higher Education within the State assignment FSRC “Crystallography and Photonics” of RAS.

Data Availability Statement: Not applicable.

Conflicts of Interest: The authors declare no conflict of interest. The funders had no role in the design of the study; in the collection, analyses, or interpretation of data; in the writing of the manuscript; or in the decision to publish the results.

References

1. Sun, D.; Towe, E. Strain-Generated Internal Fields in Pseudomorphic (In, Ga)As/GaAs Quantum Well Structures on {111} GaAs Substrates. *Jpn. J. Appl. Phys.* **1994**, *33*, 702–708. [[CrossRef](#)]
2. Vaccaro, P.O.; Tominaga, K.; Hosoda, M.; Fujita, K.; Watanabe, T. Quantum-Confined Stark Shift Due to Piezoelectric Effect in InGaAs/GaAs Quantum Wells Grown on (111)A GaAs. *Jpn. J. Appl. Phys.* **1995**, *34*, 1362–1366. [[CrossRef](#)]
3. Ilg, M.; Ploog, K.H.; Trampert, A. Lateral piezoelectric fields in strained semiconductor heterostructures. *Phys. Rev. B* **1994**, *50*, 17111–17119. [[CrossRef](#)]
4. Holmes, D.M.; Tok, E.S.; Sudijono, J.L.; Jones, T.S.; Joyce, B.A. Surface evolution in GaAs(1 1 0) homoepitaxy; from microscopic to macroscopic morphology. *J. Cryst. Growth* **1998**, *192*, 33–46. [[CrossRef](#)]
5. Yerino, C.D.; Liang, B.; Huffaker, D.L.; Simmonds, P.J.; Lee, M.L. Review Article: Molecular beam epitaxy of lattice-matched InAlAs and InGaAs layers on InP (111)A, (111)B, and (110). *J. Vac. Sci. Technol. B* **2017**, *35*, 010801. [[CrossRef](#)]
6. Cruz-Hernández, E.; Vázquez-Cortés, D.; Shimomura, S.; Méndez-García, V.H.; López-López, M. Study of the conduction-type conversion in Si-doped (631)A GaAs layers grown by molecular beam epitaxy. *Phys. Status Solidi C* **2011**, *8*, 282–284. [[CrossRef](#)]
7. Méndez-García, V.-H.; Shimomura, S.; Gorbachev, A.Y.; Cruz-Hernández, E.; Vázquez-Cortés, D. Si-doped AlGaAs/GaAs (631)A heterostructures grown by MBE as a function of the As-pressure. *J. Cryst. Growth* **2015**, *425*, 85–88. [[CrossRef](#)]
8. Tok, E.S.; Neave, J.H.; Ashwin, M.J.; Joyce, B.A.; Jones, T.S. Growth of Si-doped GaAs(110) thin films by molecular beam epitaxy; Si site occupation and the role of arsenic. *J. Appl. Phys.* **1998**, *83*, 4160–4167. [[CrossRef](#)]
9. Sun, D.; Towe, E. Molecular beam epitaxial growth of (Al,Ga)As/GaAs heterostructures and Si doping characterization study on vicinal (110) GaAs substrates. *J. Cryst. Growth* **1993**, *132*, 166–172. [[CrossRef](#)]
10. Takano, Y.; Lopez, M.; Torihata, T.; Ikei, T.; Kanaya, Y.; Pak, K.; Yonezu, H. Realization of mirror surface in (111)- and (110)-oriented GaAs by migration-enhanced epitaxy. *J. Cryst. Growth* **1991**, *111*, 216–220. [[CrossRef](#)]
11. Holmes, D.M.; Belk, J.G.; Sudijono, J.L.; Neave, J.H.; Jones, T.S.; Joyce, B.A. The nature of island formation in the homoepitaxial growth of GaAs(110). *Surf. Sci.* **1995**, *341*, 133–141. [[CrossRef](#)]
12. Tok, E.S.; Jones, T.S.; Neave, J.H.; Zhang, J.; Joyce, B.A. Is the arsenic incorporation kinetics important when growing GaAs(001), (110), and (111)A films? *Appl. Phys. Lett.* **1997**, *71*, 3278–3280. [[CrossRef](#)]
13. Wassermeier, M.; Yang, H.; Tornie, E.; Daweritz, L.; Ploog, K. Growth mechanism of GaAs on (110) GaAs studied by high—Energy electron diffraction and atomic force microscopy. *J. Vac. Sci. Technol. B* **1994**, *12*, 2574–2578. [[CrossRef](#)]
14. Holland, M.C.; Kean, A.H.; Stanley, C.R. Silicon compensation and scattering mechanisms in two-dimensional electron gases on (110) GaAs. *J. Cryst. Growth* **1995**, *150*, 455–459. [[CrossRef](#)]
15. Holmes, D.M.; Belk, J.G.; Sudijono, J.L.; Neave, J.H.; Jones, T.S.; Joyce, B.A. Different growth modes in GaAs(110) homoepitaxy. *J. Vac. Sci. Technol. A* **1996**, *14*, 849–853. [[CrossRef](#)]
16. Junming, Z.; Yi, H.; Yongkang, L.; Yi, J.W. Growth and properties of AlGaAs/GaAs heterostructures on GaAs (110) surface. *J. Cryst. Growth* **1987**, *81*, 221–223. [[CrossRef](#)]
17. Pfeiffer, L.; West, K.W.; Stormer, H.L.; Eisenstein, J.P.; Baldwin, K.W.; Gershoni, D.; Spector, J. Formation of a high quality two—Dimensional electron gas on cleaved GaAs. *Appl. Phys. Lett.* **1990**, *56*, 1697–1699. [[CrossRef](#)]
18. Simmonds, P.J.; Lee, M.L. Tensile-strained growth on low-index GaAs. *J. Appl. Phys.* **2012**, *112*, 054313. [[CrossRef](#)]
19. Iba, S.; Fujino, H.; Fujimoto, T.; Koh, S.; Kawaguchi, H. Correlation between electron spin relaxation time and hetero-interface roughness in (110)-oriented GaAs/AlGaAs multiple-quantum wells. *Phys. E Low-Dimens. Syst. Nanostruct.* **2009**, *41*, 870–875. [[CrossRef](#)]
20. Fischer, F.; Schuh, D.; Bichler, M.; Abstreiter, G.; Grayson, M.; Neumaier, K. Modulating the growth conditions: Si as an acceptor in (110) GaAs for high mobility p-type heterostructures. *Appl. Phys. Lett.* **2005**, *86*, 192106. [[CrossRef](#)]
21. Sørensen, C.B.; Gislason, H.; Hvam, J.M. MBE growth of two-dimensional electron gases on (110) GaAs. *J. Cryst. Growth* **1997**, *175–176*, 1097–1101. [[CrossRef](#)]
22. Volkl, R.; Griesbeck, M.; Tarasenko, S.A.; Schuh, D.; Wegscheider, W.; Schuller, C.; Korn, T. Spin dephasing and photoinduced spin diffusion in a high-mobility two-dimensional electron system embedded in a GaAs-(Al,Ga)As quantum well grown in the [110] direction. *Phys. Rev. B* **2011**, *83*, 241306. [[CrossRef](#)]
23. Allen, L.T.P.; Weber, E.R.; Washburn, J.; Pao, Y.C. Device quality growth and characterization of (110) GaAs grown by molecular beam epitaxy. *Appl. Phys. Lett.* **1987**, *51*, 670–672. [[CrossRef](#)]
24. Allen, L.T.P.; Weber, E.R.; Washburn, J.; Pao, Y.C.; Elliot, A.G. Characterization of surface faceting on (110)GaAs/GaAs grown by molecular beam epitaxy. *J. Cryst. Growth* **1988**, *87*, 193–200. [[CrossRef](#)]

25. Sato, M.; Maehashi, K.; Asahi, H.; Hasegawa, S.; Nakashima, H. MBE growth of AlGaAs/GaAs superlattices on GaAs (110) substrates. *Superlattices Microstruct.* **1990**, *7*, 279–282. [[CrossRef](#)]
26. Tejedor, P.; Smilauer, P.; Joyce, B.A. Growth modes in homoepitaxy on vicinal GaAs(110) surfaces. *Surf. Sci.* **1999**, *424*, L309–L313. [[CrossRef](#)]
27. Miyagawa, A.; Yamamoto, T.; Ohnishi, Y.; Nelson, J.T.; Ohachi, T. Silicon doping into MBE-grown GaAs at high arsenic vapor pressures. *J. Cryst. Growth* **2002**, *237–239*, 1434–1439. [[CrossRef](#)]
28. Zhou, T.C.; Zhou, X.C.; Kirk, W.P. A comparative study of Si doping in GaAs layers grown by molecular beam epitaxy on GaAs(110) and GaAs(001) surfaces. *J. Appl. Phys.* **1997**, *81*, 7372–7375. [[CrossRef](#)]
29. Pavesi, L.; Henini, M.; Johnston, D. Influence of the As overpressure during the molecular beam epitaxy growth of Si doped (211)A and (311)A GaAs. *Appl. Phys. Lett.* **1995**, *66*, 2846–2848. [[CrossRef](#)]
30. Agawa, K.; Hirakawa, K.; Sakamoto, N.; Hashimoto, Y.; Ikoma, T. Electrical properties of heavily Si-doped (311)A GaAs grown by molecular beam epitaxy. *Appl. Phys. Lett.* **1994**, *65*, 1171–1173. [[CrossRef](#)]
31. Okano, Y.; Shigeta, M.; Seto, H.; Katahama, H.; Nishine, S.; Fujimoto, I. Incorporation Behavior of Si Atoms in the Molecular Beam Epitaxial Growth of GaAs on Misoriented (111)A Substrates. *Jpn. J. Appl. Phys.* **1990**, *29*, L1357–L1359. [[CrossRef](#)]
32. Ballingall, J.M.; Wood, C.E.C. Crystal orientation dependence of silicon autocompensation in molecular beam epitaxial gallium arsenide. *Appl. Phys. Lett.* **1982**, *41*, 947–949. [[CrossRef](#)]
33. Galiev, G.B.; Klimov, E.A.; Zaitsev, A.A.; Pushkarev, S.S.; Klochkov, A.N. Study of the Surface Morphology, Electrophysical Characteristics, and Photoluminescence Spectra of GaAs Epitaxial Films on GaAs(110) Substrates. *Opt. Spectrosc.* **2020**, *128*, 877–884. [[CrossRef](#)]
34. Vilisova, M.D.; Kunitsyn, A.E.; Lavrent'eva, L.G.; Preobrazhenskii, V.V.; Putyato, M.A.; Semyagin, B.R.; Toropov, S.E.; Chaldyshev, V.V. Doping of GaAs layers with Si under conditions of low-temperature molecular beam epitaxy. *Semiconductors* **2002**, *36*, 953–957. [[CrossRef](#)]
35. Piazza, F.; Pavesi, L.; Henini, M.; Johnston, D. Effect of As overpressure on Si-doped (111)A GaAs grown by molecular beam epitaxy: A photoluminescence study. *Semicond. Sci. Technol.* **1992**, *7*, 1504–1507. [[CrossRef](#)]
36. Pavesi, L.; Ky, N.H.; Ganiere, J.D.; Reinhart, F.K.; Baba-Ali, N.; Harrison, I.; Tuck, B.; Henini, M. Role of point defects in the silicon diffusion in GaAs and Al_{0.3}Ga_{0.7}As and in the related superlattice disordering. *J. Appl. Phys.* **1992**, *71*, 2225–2237. [[CrossRef](#)]

Disclaimer/Publisher's Note: The statements, opinions and data contained in all publications are solely those of the individual author(s) and contributor(s) and not of MDPI and/or the editor(s). MDPI and/or the editor(s) disclaim responsibility for any injury to people or property resulting from any ideas, methods, instructions or products referred to in the content.